ACS Macro Letters

pubs.acs.org/macroletters Letter

Preparation and Characterization of Intrinsic Porous Polyamides Based on Redox-Active Aromatic Diamines with Pentiptycene Scaffolds

Min-Hao Pai, Chien-Chieh Hu,* Wei Shyang Tan, Jye-Shane Yang,* and Guey-Sheng Liou*

Cite This: ACS Macro Lett. 2021, 10, 1210−1215 Read Online

ACCESS | Metrics & More | Article Recommendations | Supporting Information

ABSTRACT: The electrochromic (EC) polyamides (**Ether-PentiTPA1** and **Ether-PentiTPA8**) from the electroactive pentiptycene-derived triphenylaminediamine monomers (**PentiTPA1** and **PentiTPA8**) were designed and prepared via polycondensation. The incorporation of rigid and contorted H-shaped pentiptycene scaffolds could restrain polymer chains from close packing and further form intrinsic microporosity in the polymer matrix which could be confirmed by the measurements of WXRD, BET, and PALS. With the existence of intrinsic microporosity, the diffusion rate of counterions between the electroactive polymer film and electrolyte can be promoted during the electrochemical procedure. Therefore, the prepared polyamide **Ether-PentiTPA1** exhibits enhanced EC behaviors, such as lower driving potential (1.11 V), smaller redox potential difference ΔE (0.24 V), and shorter switching response time (3.6/5.2 s for coloring/bleaching). Consequently, the formation of intrinsic microporosity can be a useful approach for the enhancement of EC response performance.

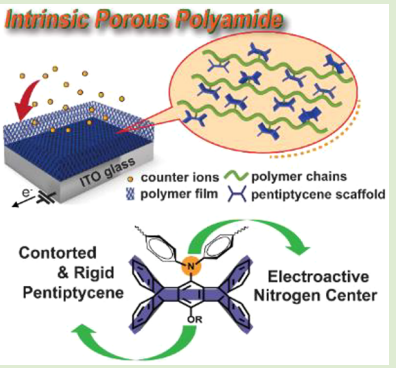

With the development of technology and diverse demands from mature customers, various optoelectronic materials are explored and sprung up. Among them, electrochromic (EC) materials with a reversible change in optical transmittance during the redox procedure have been in the spotlight and studied for decades[1,2] because of their obvious optical contrast ratio, fast response capability, high coloration efficiency, and so on. Since 2005, our research group has concentrated on the development of triphenylamine (TPA)-based polyamides and polyimides with various substituents to investigate the EC behaviors.[3,4] The outcomes reveal that the TPA-derived polymer system is one of the most potential candidates for the application of displays and novel optical devices due to the features of high transparency in the neutral state, good flexibility, outstanding thermal stability, and distinguished electrochemical properties. Moreover, TPA-based electroactive polymers possess excellent processing ability because of the good solubility caused by the special propeller-shaped conformation of the TPA moiety which is beneficial for the fabrication of electrochromic devices (ECDs).

However, the balance among the optical contrast ratio, driving potential, and response capability remains a challenge in practical application.[5] Generally, the thicker EC films could exhibit a higher optical contrast ratio but show poorer response capability and higher driving potential in the meantime. In our previous research, the porous polymer films formed by washing out the additional salts could effectively increase the surface area and generate channels throughout the whole polymer film that could facilitate the transport of counterions of electrolytes during the redox procedure.[6,7] However, oversized pores would decrease the transmittance of polymer films at the neutral state and thus reduce the contrast ratio at the oxidative state. As a result, polymers of intrinsic microporosity (PIMs) with much-reduced pore size are expected to be a judicious approach for enhancing the EC response capability without sacrificing the optical properties.

The concept of PIMs was first proposed and developed from the phthalocyanine materials by McKeown during the 1990s.[8,9] In general, PIMs could possess a large amount of void space by designing polymers with rigid and contorted structures, such as spirobifluorene (SBF),[10−12] ethanoanthracene (EA),[12−15] and Tröger's base,[14,16,17] to prevent polymer chains from efficient packing. In this context, iptycenes such as triptycene (Y-shaped) and pentiptycene (H-shaped)[18] are attractive structural units for PIMs due to the presence of internal molecular free volume (IMFV), that is, the unoccupied volume of concavities of the iptycene units relative to the total volume of polymers.[19] The IMFV feature of iptycenes has been applied in various fields, such as gas separation membrane,[20,21] low-*K*

Received: July 24, 2021
Accepted: September 17, 2021

https://doi.org/10.1021/acsmacrolett.1c00487
ACS Macro Lett. 2021, 10, 1210−1215

Scheme 1. Synthetic Routes of the Prepared Polyamides

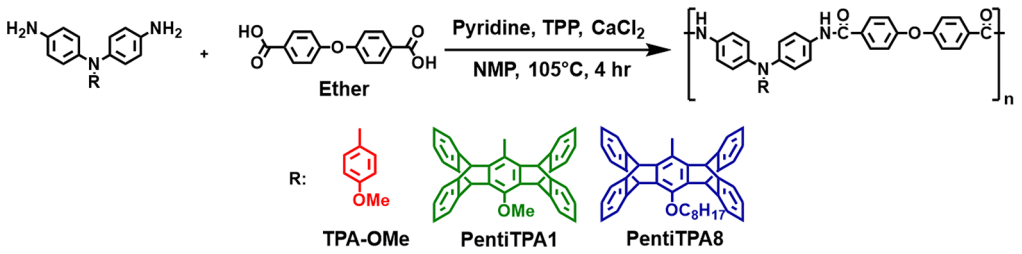

dielectric materials,[22] optical materials (liquid crystals),[19] and chemical detector.[23]

Recently, our groups incorporated the nonelectroactive pentiptycene scaffolds into the polymer chain to enhance the response capability and to lower the driving potential of the corresponding EC films. We proposed that the U- and V-shaped cavities of the pentiptycene scaffolds could effectively produce IMFV to generate the intrinsic microporosity and to facilitate the diffusion of counterions in electrolytes during the redox procedure.[24] In addition, because of the molecular clipping effect of polymer chain threading through the pentiptycene cavities, the electrochemical capacity and stability of the pentiptycene-containing polymer films could be enhanced.[25]

Herein, we report the synthesis and EC properties of two new pentiptycene-containing and TPA-based polyamides **Ether-PentiTPA1** and **Ether-PentiTPA8**, as shown in Scheme 1. The structure−property relationship and the effects of the pentiptycene scaffolds are elucidated in this study. A schematic diagram of the fabrication of ECDs is depicted in Figure S1.

Two pentiptycene-derived TPA diamine monomers **PentiTPA1** (compound **4**) and **PentiTPA8** (compound **7**) were successfully prepared via the procedures as depicted in Scheme S1. NMR, FTIR, and high-resolution mass spectrometry (HRMS) were used to identify the structures of intermediate products and pentiptycene-based diamine monomers as provided in Figures S2−S15 (^{1}H and ^{13}C NMR spectra). The conformational rigidity of these TPA diamine monomers was simulated via energy variation as a function of the dihedral angle at the rotation centers. According to the results illustrated in Figure 1a, the optimum dihedral angle is ∼65° for **PentiTPA1** and **PentiTPA8** but ∼40° for **TPA-OMe**. Moreover, the energy surface is deep for both **PentiTPA1** and **PentiTPA8** but rather shallow for **TPA-OMe**, indicating that the pentiptycene scaffolds impose a significant conformational rigidity to the TPA diamine.[26] Consequently, the solubility and optical transparency of the prepared polyamide films could be enhanced as shown in the following. Also, the three different TPA-based polyamides were synthesized from three kinds of TPA diamine monomers with 4,4′-oxidibenzoic acid via direct solution polycondensation as illustrated in Scheme 1. The NMR spectra and FTIR spectra were utilized to identify the structures of these obtained polyamides as shown in Figures S16−S19.

The molecular weights, PDI, and solubility behaviors of the three polyamides are summarized in Tables S1 and S2. All three polyamides exhibit excellent solubility in common polar aprotic organic solvents such as DMSO and DMAc and sufficiently high molecular weight (M_n > 15000) for forming flexible films (thickness: 25 ± 5 μm) as demonstrated in Figure S20. The thermal properties were investigated by TMA and TGA as depicted in Figures S21 and S22, respectively, and the

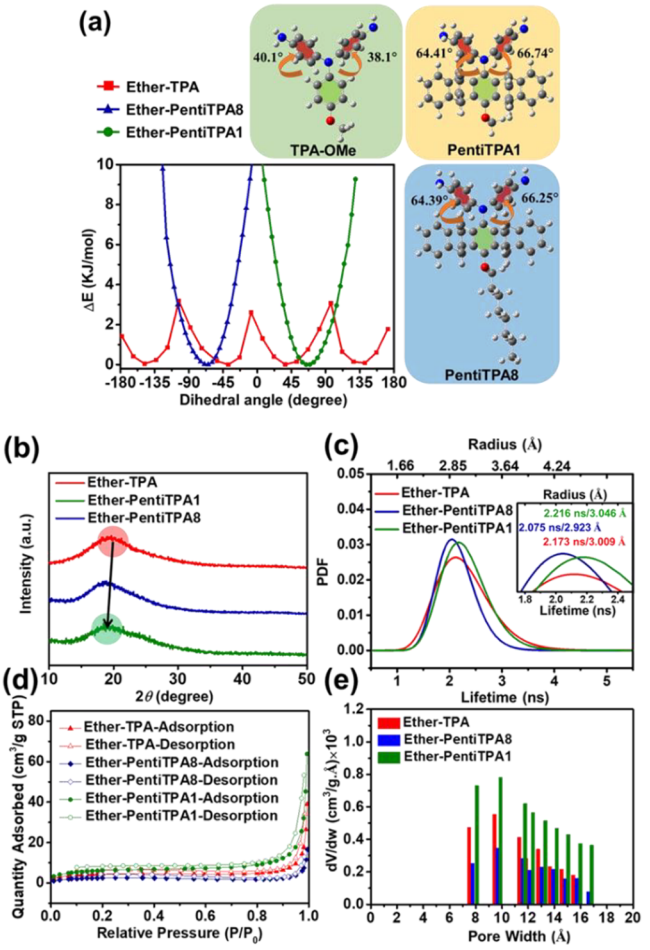

Figure 1. (a) Energy-minimized conformations and the relationship between energy and dihedral angle of **TPA-OMe**, **PentiTPA1**, and **PentiTPA8** calculated by B3LYP/6-31G(d). (b) WXRD patterns of the polyamide films (thickness: 25 ± 5 μm). (c) PALS analysis and calculated free volume size. (d) N_2 adsorption (filled) and desorption (empty) isotherms measured at 77 K. (e) Pore width distributions analyzed by nitrogen adsorption at 77 K via the Horvath−Kawazoe method.

results are summarized in Table S3. All the polyamides possess outstanding thermal stability without weight loss up to 300 °C in TGA measurements under both air and nitrogen atmospheres. Besides, with the increased fraction of the pentiptycene scaffold in the polymer chains, the softening temperature (T_s) of **Ether-PentiTPA1** boosts up to 375 °C, indicating that the rigid and contorted **PentiTPA1** units could effectively increase the stiffness of the polymer and prevent polymer chains from efficient packing.

To investigate the intrinsic microporosity of the polyamides caused by the pentiptycene scaffolds, measurements including

https://doi.org/10.1021/acsmacrolett.1c00487
ACS Macro Lett. 2021, 10, 1210−1215

Table 1. Characteristic of Intrinsic Microporosity in Polyamides

polymers	S_{BET} (m^2/g)[a]	2θ (deg)[b]	d (Å)[c]	ρ (g/cm^3)	τ_3 (ns)[d]	R (Å)[e]	FFV[f]
Ether-TPA	16	19.65	4.51	1.193	2.173	3.009	0.1376
Ether-PentiTPA8	10	18.93	4.68	1.063	2.075	2.923	0.2546
Ether-PentiTPA1	26	18.44	4.81	0.972	2.216	3.046	0.3254

[a]Calculated by the results of the N2 adsorption (filled) and desorption (empty) isotherms measured by BET at 77 K. [b]Measured by WXRD at the scan range of 2θ from 10° to 50°. [c]Calculated from the result of the WXRD curve by Bragg's law. [d]The o-Ps lifetime measured by PALS. [e]The mode radius of free volume size calculated by the result of o-Ps lifetime. [f]Fractional free volume was calculated by equation related to the density and van der Waals molar volume as shown in the Supporting Information.

WXRD, PALS, Brunauer–Emmett–Teller (BET) surface areas, and density were conducted. The results are illustrated in Figure 1b–e and summarized in Table 1. The WXRD data provide information about the behavior of polymer chain aggregation. All the polyamide films show a broad diffraction pattern with peaks around 19° in the WXRD as illustrated in Figure 1b, indicating the presence of some ordered domain in the amorphous polymer matrixes. The calculated d-spacing values for **Ether-TPA**, **Ether-PentiTPA8**, and **Ether-PentiTPA1** are 4.51, 4.68, and 4.81 Å, respectively, which could be assigned to the interchain distance between the polymer chains in the out-of-plane direction.[27]

Besides, PALS was used to investigate the free volume size of the prepared polymer films. PALS mainly measures positronium (Ps) annihilation lifetimes and intensities to calculate the size and amount of vacancy in materials, such as voids or pores in the range from several angstroms to 10 nm.[28] The positron lifetime τ_3 is generally from the triple-state (ortho-Ps), which prefers to stay in defects or pores and can be annihilated by interaction with molecular electrons during collisions to the pore surface.

Consequently, the value of τ_3 reflects the pore size. The τ_3 values for **Ether-TPA**, **Ether-PentiTPA8**, and **Ether-PentiTPA1** are 2.173, 2.075, and 2.216 ns, corresponding to the free volume radius of 3.009, 2.923, and 3.046 Å, respectively, as depicted in Figure 1c. Accordingly, **Ether-PentiTPA1** possesses a higher free volume probability density function (PDF) than **Ether-TPA** in the radius range of around 2.85–3.64 Å, and **Ether-PentiTPA8** has the lowest PDF value. In other words, the pentiptycene groups could efficiently prevent polymer chains from close packing to facilitate the formation of intrinsic microporosity. However, in the presence of long alkyl chains as in **Ether-PentiTPA8** the pentiptycene effect is counterbalanced, presumably due to the threading of the alkyl chain through the pentiptycene cavities.[29]

Moreover, the BET isotherms of the polyamides determined by nitrogen adsorption/desorption at 77 K are depicted in Figure 1d. The estimated BET surface area is almost 2 times larger in **Ether-PentiTPA1** (26 m^2/g) than in **Ether-TPA** (16 m^2/g), attributable to the increased microporosity caused by the pentiptycene units. The pore width distributions analyzed by nitrogen adsorption at 77 K via the Horvath–Kawazoe method are displayed in Figure 1e. **Ether-PentiTPA1** possesses more micropores (<2 nm) than the other two polyamides, consistent with the outcomes of PALS. In addition, the densities of **Ether-TPA**, **Ether-PentiTPA1**, and **Ether-PentiTPA8** films were also measured by an analytical balance fitted with a Mettler density kit in 2,2,4-trimethylpentane. The pentiptycene-containing polyamides exhibit a lower density, and in particular **Ether-PentiTPA1** displays the lowest density of 0.937 g/cm^3, which is much lower than the corresponding **Ether-TPA** (1.193 g/cm^3). Also, **Ether-PentiTPA1** (FFV = 0.3254) possesses the highest fractional free volume (FFV) calculated by the density and van der Waals mole volume. In summary, among the three polyamide films, **Ether-PentiTPA1** has the largest d-spacing and free volume size as well as the highest number of pores and surface area. Consequently, the incorporation of rigid and bulky pentiptycene scaffolds into the redox-active polymers is an effective approach to create intrinsic microporosity in polyamide films.

The optical transparency of polyamide films coating on the glass slide and ITO glasses with the thickness of 25 ± 5 μm (thick polymer films) and 600–700 nm (thin polymer films), respectively, was measured by UV–vis spectroscopy. As shown in Figures S23 and S24, all the polyamide films exhibit high transparency in the visible region. Intriguingly, **Ether-PentiTPA1** and **Ether-PentiTPA8** display nearly colorless appearance that could be attributed to the suppression of interchain charge transfer (ICT) by the sterically hindered pentiptycene units. The thin polyamide films coated on ITO glass with a thickness of 600–700 nm shown in Figure S25 exhibit excellent transparency over the visible region which is more beneficial for practical applications.

The electrochemical behavior of the prepared polyamide films coated on ITO was investigated by cyclic voltammetry (CV). The CV diagrams are depicted in Figure 2a, and the

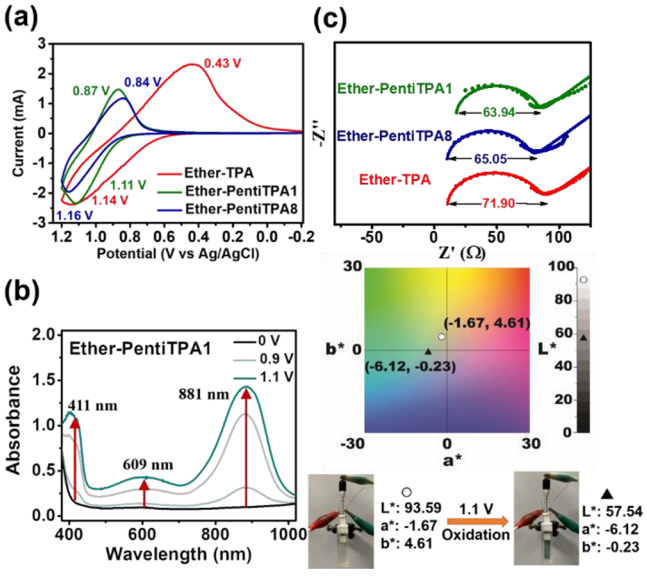

Figure 2. (a) Cyclic voltammetric diagrams of **Ether-TPA**, **Ether-PentiTPA1**, and **Ether-PentiTPA8** measured on the ITO-coated glass substrate in 0.1 M $TBABF_4$/MeCN at a scan rate of 50 mV/s. (b) Spectroelectrochemical spectra and the CIELAB color space for **Ether-PentiTPA1** (thickness: 660 ± 50 nm) measured on the ITO-coated glass substrate in 0.1 M $TBABF_4$/MeCN. (c) Nyquist plots of the polyamide films under oxidation state.

https://doi.org/10.1021/acsmacrolett.1c00487
ACS Macro Lett. 2021, 10, 1210–1215

results are listed in Table 2. All these three TPA-based polyamides exhibited one reversible oxidation redox peak, and the oxidation potential is lower for **Ether-PentiTPA1** (1.11 V) than **Ether-TPA** (1.14 V) and **Ether-PentiTPA8** (1.16 V). Moreover, ΔE, the potential difference between the oxidation and the reduction peaks, can be used to evaluate the transfer rate of electrons during electrochemical processes. In general, smaller ΔE indicates the higher transfer rate of electrons and a lower driving force are necessary to switch the redox procedure, which could be advantageous to enhance EC behaviors with a shorter switching time.

Table 2. Electrochemical Parameters of Prepared Polyamide Films

films	E_{oxi} (V)[a]	E_{red} (V)[b]	ΔE (V)[c]	R_{ct} (Ω)[d]
Ether-TPA (620 ± 20 nm)	1.14	0.43	0.71	71.90
Ether-PentiTPA8 (650 ± 50 nm)	1.16	0.84	0.32	65.05
Ether-PentiTPA1 (660 ± 50 nm)	1.11	0.87	0.24	63.94

[a]Oxidation potential at the peak. [b]Reduction potential at the peak. [c]Potential difference between oxidation and reduction peaks, $|E_{oxi} - E_{red}|$. [d]Obtained from the diameter of the semicircle or the arc.

Accordingly, a lower ΔE for **Ether-PentiTPA1** (0.24 V) than **Ether-TPA** (0.71 V) and **Ether-PentiTPA8** (0.32 V) indicates a positive influence of pentiptycene scaffold on the performance of electrochemical behavior. This might be attributed to the bulky and rigid pentiptycene units that prevent polymer chains from close packing to generate intrinsic microporosity, which in turn facilitates the diffusion of the counterions in the polymer films.

The spectroelectrochemical spectra and related L, a^*, and b^* values of **Ether-TPA** film are illustrated in Figure S26. At the onset, the **Ether-TPA** film revealed a very pale-yellow color at the neutral state (0 V); the intensity of the characteristic peaks at 430 and 796 nm gradually raised, and the polymer film turned to green with increasing applied potential. As shown in Figure 2b and Figure S27, the spectroelectrochemical spectra and related L, a^*, and b^* values of **Ether-PentiTPA1** and **Ether-PentiTPA8** films, respectively, display a similar tendency. Both polyamide films showed a transparent pale yellow at the neutral state (0 V); then the intensity of characteristic peaks at 411, 609, and 881 nm was increased with increasing the applied potential, and the films changed to a dark-green color. In addition, **Ether-PentiTPA1** also exhibited good EC stability for 50 cycles as illustrated in Figure S28.

As a crucial parameter for the redox-active EC materials, the switching response time could be evaluated by monitoring the characteristic absorption peak as a function of time at a specific applying potential. The results of the switching test for the electroactive polyamide films of **Ether-TPA**, **Ether-PentiTPA1**, and **Ether-PentiTPA8** are depicted in Figure S29 and summarized in Table 3. Herein, the monitored wavelength for **Ether-TPA** was 796 nm, while that for **Ether-PentiTPA1** and **Ether-PentiTPA8** was 881 nm based on the results of spectroelectrochemical spectra. The applied potentials were set at 1.15 and −0.1 V for coloring and bleaching, respectively. According to the results, **Ether-PentiTPA1** displayed the lowest response time of 3.6 and 5.2 s for coloring and bleaching, respectively. This again could be attributed to the intrinsic microporosity that facilitates the diffusion of the counterions during the redox procedure. Consequently, the coloring time of **Ether-PentiTPA8** and **Ether-PentiTPA1** could be reduced by 25% and 49%, while the bleaching time of **Ether-PentiTPA8** and **Ether-PentiTPA1** could be further decreased by 12% and 27% when compared to **Ether-TPA**. Furthermore, the coloration efficiency of the prepared polymer films was calculated as shown in Table S4 and Figure S30. **Ether-PentiTPA1** (170.8 cm^2/C) exhibited a higher coloration efficiency than **Ether-PentiTPA8** (121.2 cm^2/C) and **Ether-TPA** (119.4 cm^2/C), indicating that **Ether-PentiTPA1** could reach a high contrast ratio with less current consumption.

Table 3. Switching Response of Prepared Polyamide Films

films	t_c (s)[a]	Δt_c (s)[b]	Δt_c (%)[c]	t_b (s)[d]	Δt_b (s)[e]	Δt_b (%)[f]
Ether-TPA (620 ± 20 nm)	4.8			10.3		
Ether-PentiTPA8 (650 ± 50 nm)	4.2	0.6	12.5	7.5	2.8	27.2
Ether-PentiTPA1 (660 ± 50 nm)	3.6	1.2	25.0	5.2	5.1	49.5

[a]Coloring time from a neutral state to 90% of optical change. [b]The difference in coloring time compared with **Ether-TPA**. [c]The percentage of decreasing coloring time compared with **Ether-TPA**. [d]Bleaching time from coloring state to 90% of optical change. [e]The difference of bleaching time compared with **Ether-TPA**. [f]The percentage of decreasing bleaching time compared with **Ether-TPA**.

In addition, electrochemical impedance spectroscopy (EIS) was utilized to study the electroactivity and conductivity of the polyamide films coated on ITO glass, and the obtained Nyquist plots fitted by a Randles circuit are shown in Figure 2c with data summarized in Table 2. During the oxidation processes, the transfer resistance (R_{ct}) values of **Ether-TPA**, **Ether-PentiTPA8**, and **Ether-PentiTPA1** are 71.90, 65.05, and 63.94 Ω, respectively. The lowest R_{ct} **Ether-PentiTPA1** is consistent with the claim of enhanced counterions transportation during the redox process.

To further confirm the relative performance in devices, polyamides of **Ether-TPA** and **Ether-PentiTPA1** were chosen to fabricate ECDs with HV in a gel-type electrolyte system.[30] The CV diagrams of the devices are depicted in Figure S31, and the corresponding values are summarized in Table S5. The ΔE of the ECD derived from **Ether-PentiTPA1/HV** (0.20 V) is lower than that from **Ether-TPA/HV** (0.28 V), confirming again that **Ether-PentiTPA1** is superior to **Ether-TPA** as the EC materials. Furthermore, it is worth noting that the ΔE is smaller for ECDs than that of the cases related to just EC films because of the help of HV. The spectroelectrochemical spectra and related L, a^*, and b^* values of **Ether-TPA/HV** and **Ether-PentiTPA1/HV** ECDs during the electrochemical processes are shown in Figures S32 and S33, respectively. The optical absorption spectra of the ECDs display similar characteristic absorption patterns as those of their related polymer films as illustrated in Figure S26 and Figure 2b and show an additional HV^+ characteristic absorption peak at around 603 nm while increasing the applied switching on potential.

The switching response of ECDs was also evaluated, and as in the case of polymer films, the monitored wavelengths were 796 and 881 nm for **Ether-TPA/HV** and **Ether-PentiTPA1/HV**, respectively. The results are depicted in Figure S34 and summarized in Table S6. While the coloring and bleaching

https://doi.org/10.1021/acsmacrolett.1c00487
ACS Macro Lett. 2021, 10, 1210−1215

response times for the **Ether-TPA/HV** ECD are 8.8 and 32.3 s, respectively, they are 8.4 and 25.6 s for **Ether-PentiTPA1/HV**, which confirm the pentiptycene effect (intrinsic microporosity) on the enhancement of response capability of TPA-based polyamides in the ECD system.

In summary, the pentiptycene-containing polyamides (**Ether-PentiTPA1** and **Ether-PentiTPA8**) have been successfully synthesized from the polycondensation of the electroactive pentiptycene-based TPA diamines (**PentiTPA1** and **PentiTPA8**) and 4,4′-oxidibenzoic acid. They exhibit excellent solubility in common polar aprotic solvents and possess outstanding thermal stability. In particular, **Ether-PentiTPA1** demonstrates the best EC behaviors among these polyamide films, including the lowest oxidation potential (1.11 V), the smallest ΔE (0.24 V), and the shortest switching response time (3.6/5.2 s for coloring and bleaching) during the oxidation procedure, which could be attributed to the presence of intrinsic microporosity that facilitates the counterions diffusion of electrolytes. Consequently, the approach of polymers of intrinsic microporosity (PIMs) is useful not only in the field of gas separation but also in the redox-active EC materials.

■ ASSOCIATED CONTENT

Supporting Information

The Supporting Information is available free of charge at https://pubs.acs.org/doi/10.1021/acsmacrolett.1c00487.

Additional experimental details, materials, and methods; NMR spectra for all compounds and polyamides; FTIR, TMA, TGA, and UV−vis spectra of polyamides; spectroelectrochemical spectra of polyamide films and ECDs (PDF)

■ AUTHOR INFORMATION

Corresponding Authors

Guey-Sheng Liou − *Institute of Polymer Science and Engineering, National Taiwan University, Taipei 10617, Taiwan;* orcid.org/0000-0003-3725-3768; Phone: +886-2-33665070; Email: gsliou@ntu.edu.tw

Chien-Chieh Hu − *Graduate Institute of Applied Science and Technology, National Taiwan University of Science and Technology, Taipei 106335, Taiwan;* orcid.org/0000-0002-3379-1764; Email: cchu@mail.ntust.edu.tw

Jye-Shane Yang − *Department of Chemistry, National Taiwan University, Taipei 10617, Taiwan;* orcid.org/0000-0003-4022-2989; Email: jsyang@ntu.edu.tw

Authors

Min-Hao Pai − *Institute of Polymer Science and Engineering, National Taiwan University, Taipei 10617, Taiwan*

Wei Shyang Tan − *Department of Chemistry, National Taiwan University, Taipei 10617, Taiwan*

Complete contact information is available at: https://pubs.acs.org/10.1021/acsmacrolett.1c00487

Author Contributions

M-H.P. and W.S.T. contributed equally to this work.

Notes

The authors declare no competing financial interest.

■ ACKNOWLEDGMENTS

This work received financial support from the Ministry of Science and Technology in Taiwan (MOST 107-2113-M-002-022-MY3, 107-2113-M-002-024-MY3, and 107-2221-E-002-066-MY3). We appreciate Ying-Feng Hsu and Samala Venkateswarlu at the Department of Chemistry, National Taiwan University, for valuable discussions and synthesis of diamine monomers, respectively. Besides, we gratefully thank Shou-Ling Huang and Ching-Wei Lu for the assistance in NMR experiments and EA measurements, respectively, of the Instrumentation Center at NTU which is supported by the Ministry of Science and Technology, Taiwan.

■ REFERENCES

(1) Deb, S. A novel electrophotographic system. *Appl. Opt.* **1969**, *8* (101), 192−195.

(2) Platt, J. R. Electrochromism, a possible change of color producible in dyes by an electric field. *J. Chem. Phys.* **1961**, *34* (3), 862−863.

(3) Yen, H. J.; Liou, G. S. Recent advances in triphenylamine-based electrochromic derivatives and polymers. *Polym. Chem.* **2018**, *9* (22), 3001−3018.

(4) Chiu, K. Y.; Su, T. X.; Li, J. H.; Lin, T. H.; Liou, G. S.; Cheng, S. H. Novel trends of electrochemical oxidation of amino-substituted triphenylamine derivatives. *J. Electroanal. Chem.* **2005**, *575* (1), 95−101.

(5) Liu, H. S.; Pan, B. C.; Huang, D. C.; Kung, Y. R.; Leu, C. M.; Liou, G. S. Highly transparent to truly black electrochromic devices based on an ambipolar system of polyamides and viologen. *NPG Asia Mater.* **2017**, *9* (6), e388−e388.

(6) Pan, B. C.; Chen, W. H.; Hsiao, S. H.; Liou, G. S. A facile approach to prepare porous polyamide films with enhanced electrochromic performance. *Nanoscale* **2018**, *10* (35), 16613−16620.

(7) Chiu, Y. W.; Pai, M. H.; Liou, G. S. Facile Approach of Porous Electrochromic Polyamide/ZrO2 Films for Enhancing Redox Switching Behavior. *ACS Appl. Mater. Interfaces* **2020**, *12* (31), 35273−35281.

(8) McKeown, N. B. *Phthalocyanine Materials: Synthesis, Structure and Function*; Cambridge University Press: 1998.

(9) McKeown, N. B. Polymers of intrinsic microporosity. *ISRN Mater. Sci.* **2012**, *2012*, 1.

(10) Bezzu, C. G.; Carta, M.; Tonkins, A.; Jansen, J. C.; Bernardo, P.; Bazzarelli, F.; McKeown, N. B. A spirobifluorene-based polymer of intrinsic microporosity with improved performance for gas separation. *Adv. Mater.* **2012**, *24* (44), 5930−5933.

(11) Ma, X.; Salinas, O.; Litwiller, E.; Pinnau, I. Novel spirobifluorene-and dibromospirobifluorene-based polyimides of intrinsic microporosity for gas separation applications. *Macromolecules* **2013**, *46* (24), 9618−9624.

(12) Bezzu, C. G.; Carta, M.; Ferrari, M.-C.; Jansen, J. C.; Monteleone, M.; Esposito, E.; Fuoco, A.; Hart, K.; Liyana-Arachchi, T. P.; Colina, C. M.; McKeown, N. B. The synthesis, chain-packing simulation and long-term gas permeability of highly selective spirobifluorene-based polymers of intrinsic microporosity. *J. Mater. Chem. A* **2018**, *6* (22), 10507−10514.

(13) Emmler, T.; Heinrich, K.; Fritsch, D.; Budd, P. M.; Chaukura, N.; Ehlers, D.; Rätzke, K.; Faupel, F. Free volume investigation of polymers of intrinsic microporosity (PIMs): PIM-1 and PIM1 copolymers incorporating ethanoanthracene units. *Macromolecules* **2010**, *43* (14), 6075−6084.

(14) Carta, M.; Malpass-Evans, R.; Croad, M.; Rogan, Y.; Jansen, J. C.; Bernardo, P.; Bazzarelli, F.; McKeown, N. B. An efficient polymer molecular sieve for membrane gas separations. *Science* **2013**, *339* (6117), 303−307.

(15) Tocci, E.; De Lorenzo, L.; Bernardo, P.; Clarizia, G.; Bazzarelli, F.; Mckeown, N. B.; Carta, M.; Malpass-Evans, R.; Friess, K.; Pilnáček, K. T.; et al. Molecular Modeling and Gas Permeation Properties of a Polymer of Intrinsic Microporosity Composed of Ethanoanthracene and Tröger's Base Units. *Macromolecules* **2014**, *47* (22), 7900−7916.

(16) Carta, M.; Malpass-Evans, R.; Croad, M.; Rogan, Y.; Lee, M.; Rose, I.; McKeown, N. B. The synthesis of microporous polymers using Tröger's base formation. *Polym. Chem.* **2014**, *5* (18), 5267−5272.
(17) Carta, M.; Croad, M.; Jansen, J. C.; Bernardo, P.; Clarizia, G.; McKeown, N. B. Synthesis of cardo-polymers using Tröger's base formation. *Polym. Chem.* **2014**, *5* (18), 5255−5261.
(18) Yang, J. S.; Yan, J. L. Central-Ring Functionalization and Application of the Rigid, Aromatic, and H-Shaped Pentiptycene Scaffold. *Chem. Commun.* **2008**, *13*, 1501−1512.
(19) Long, T. M.; Swager, T. M. Minimization of free volume: Alignment of triptycenes in liquid crystals and stretched polymers. *Adv. Mater.* **2001**, *13* (8), 601−604.
(20) Ghanem, B. S. A facile synthesis of a novel triptycene-containing A−B monomer: precursor to polymers of intrinsic microporosity. *Polym. Chem.* **2012**, *3* (1), 96−98.
(21) Ghanem, B. S.; Swaidan, R.; Litwiller, E.; Pinnau, I. Ultra-microporous triptycene-based polyimide membranes for high-performance gas separation. *Adv. Mater.* **2014**, *26* (22), 3688−3692.
(22) Long, T. M.; Swager, T. M. Molecular design of free volume as a route to low-κ dielectric materials. *J. Am. Chem. Soc.* **2003**, *125* (46), 14113−14119.
(23) Yang, Y. S.; Swager, T. M. Fluorescent Porous Polymer Films as TNT Chemosensors: Electronic and Structural Effects. *J. Am. Chem. Soc.* **1998**, *120* (46), 11864−11873.
(24) Chiu, Y. W.; Tan, W. S.; Yang, J. S.; Pai, M. H.; Liou, G. S. Electrochromic Response Capability Enhancement with Pentiptycene-Incorporated Intrinsic Porous Polyamide Films. *Macromol. Rapid Commun.* **2020**, *41* (12), 2000186.
(25) Tan, W. S.; Lee, T. Y.; Hsu, Y. F.; Huang, S. J.; Yang, J. S. Iptycene substitution enhances the electrochemical activity and stability of polyanilines. *Chem. Commun.* **2018**, *54* (43), 5470−5473.
(26) Hu, X.; Lee, W. H.; Zhao, J.; Bae, J. Y.; Kim, J. S.; Wang, Z.; Yan, J.; Zhuang, Y.; Lee, Y. M. Tröger's Base (TB)-containing polyimide membranes derived from bio-based dianhydrides for gas separations. *J. Membr. Sci.* **2020**, *610*, 118255.
(27) Zhuang, Y.; Seong, J. G.; Do, Y. S.; Jo, H. J.; Cui, Z.; Lee, J.; Lee, Y. M.; Guiver, M. D. Intrinsically microporous soluble polyimides incorporating Tröger's base for membrane gas separation. *Macromolecules* **2014**, *47* (10), 3254−3262.
(28) Gidley, D. W.; Peng, H. G.; Vallery, R. S. Positron annihilation as a method to characterize porous materials. *Annu. Rev. Mater. Res.* **2006**, *36*, 49−79.
(29) Tsui, N. T.; Paraskos, A. J.; Torun, L.; Swager, T. M.; Thomas, E. L. Minimization of internal molecular free volume: a mechanism for the simultaneous enhancement of polymer stiffness, strength, and ductility. *Macromolecules* **2006**, *39* (9), 3350−3358.
(30) Wu, J. H.; Liou, G. S. High-Performance Electrofluorochromic Devices Based on Electrochromism and Photoluminescence-Active Novel Poly (4-Cyanotriphenylamine). *Adv. Funct. Mater.* **2014**, *24* (41), 6422−6429.

https://doi.org/10.1021/acsmacrolett.1c00487
ACS Macro Lett. 2021, 10, 1210−1215